Mercury Telluride Colloidal Quantum Dots: Electronic Structure, Size-Dependent Spectra, and Photocurrent Detection up to 12 μm

Sean E. Keuleyan,[†] Philippe Guyot-Sionnest,[*,†] Christophe Delerue,[‡] and Guy Allan[‡]

[†]James Franck Institute, University of Chicago, 929 East 57th Street, Chicago, Illinois 60637, United States, and [‡]IEMN, Dept ISEN, 41 boulevard Vauban, 59046 Lille Cedex, France

ABSTRACT HgTe colloidal quantum dots are synthesized with high monodispersivity with sizes up to ~15 nm corresponding to a room temperature absorption edge at ~5 μm. The shape is tetrahedral for larger sizes and up to five peaks are seen in the absorption spectra with a clear size dependence. The size range of the HgTe quantum dots is extended to ~20 nm using regrowth. The corresponding room temperature photoluminescence and absorption edge reach into the long-wave infrared, past 8 μm. Upon cooling to liquid nitrogen temperature, a photoconductive response is obtained in the long-wave infrared region up to 12 μm. Configuration-interaction tight-binding calculations successfully explain the spectra and the size dependence. The five optical features can be assigned to sets of single hole to single electron transitions whose strengths are strongly influenced by the multiband/multiorbital character of the quantum-dot electronic states.

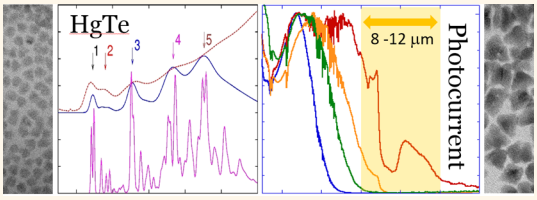

KEYWORDS: colloidal quantum dots · infrared · LWIR · photodetectors · synthesis · electronic structure

The two spectral ranges of primary interest for thermal imaging are the midwave infrared (MWIR, 3−5 μm) and the long-wave infrared (LWIR, 8−12 μm), which are the regions of atmospheric transparency. The dominant photon detectors in these ranges are single-crystal InSb and HgCdTe, while alternatives based on epitaxial quantum dot infrared photodetectors (QDIP), quantum well (QWIP), and type-II superlattices of III−V semiconductors are receiving increasing attention.[1] The costs of these materials, however, remain high. Thermal detectors are cheaper but afford a fundamentally lower detectivity and slower response compared to quantum detectors.[1] Colloidal quantum dots (CQDs) may provide an alternative, combining the advantages of speed and detectivity of quantum detectors along with much reduced fabrication costs compared to single crystal or epitaxial materials. CQDs of the semimetal HgTe have already been used as photodetectors in the near-infrared[2−4] and the mid-infrared with detection up to 7 μm at low temperature.[5] It is of interest to further investigate this promising material to expand the spectral range of detection and to develop a better understanding of the electronic structure of these quantum dots. In this work, the HgTe CQDs synthesis is improved such that they show size-dependent spectra with multiple features for particles of sizes below ~15 nm and the particle size is extended to 20 nm allowing LWIR photodetection. Tight binding calculations[6] are performed to make a detailed comparison with experiment, providing an excellent agreement in the size range corresponding to the MWIR.

RESULTS AND DISCUSSION

Experimental Details. *Monodisperse HgTe.* The previously reported synthesis of HgTe CQDs led to spectra with at most two resolved features.[7] Minor modifications of the synthesis allow in fact much better resolved spectra. The improvement comes primarily from initial dilution of the 1 M TOP:Te precursor with oleylamine. While a small injection volume may help achieve a discrete nucleation event, it appears that the relatively high reactivity, as seen by the

* Address correspondence to pgs@uchicago.edu.

Received for review July 11, 2014 and accepted August 12, 2014.

Published online August 12, 2014
10.1021/nn503805h

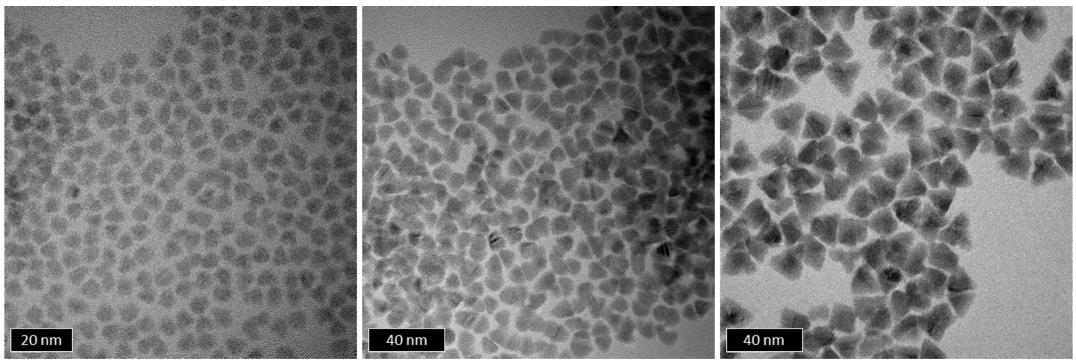

Figure 1. TEM images of 5.5, 9.1, and 15.5 nm particles.

immediate color change of the solution, likely meant that the reaction depended too greatly on mixing, where local high concentrations governed particle growth. A diluted Te precursor allows a more homogeneous mixture to form before appreciable growth has occurred while at the same time lowering the temperature sufficiently to prevent additional nucleation. Figure 1 shows TEM images of three particle sizes obtained by varying the growth temperature and time. The particles are compact and well separated on the TEM grids, in contrast to previous results where particles with similar energy gaps showed elongated and branched shapes.[8] The particles are somewhat angular at small sizes and appear clearly tetrahedral at larger sizes with partially rounded tips.

Given the nonspherical particle shape, the size is defined in this work as a shortest length between an apex and the opposite base. For the larger particles which appear with a triangular projection with slightly rounded tips, this is a better defined measure of size than the edge length. For the smaller particles which are more spherical, this definition of size evolves into the diameter.

Although the improvement in monodispersivity by this modified synthesis is not readily apparent in the TEM image due to the different projections, it is most evident in the many excitonic features now seen in the absorption spectra in Figure 2a. Prior work could resolve at most two features in the absorption spectra where up to five features are now seen. These highly resolved spectra are strongly reminiscent of the spectra of monodisperse CdSe nanoparticles in the visible region.[9] Figure 2b shows the size dependence of the PL energy. The standard deviation on the size in Figure 2b is indicated as a horizontal error bar. For the standard deviation of the size, the finite contrast of the TEM, the size distribution, and possible different projections of the particles on the TEM grid all contribute. The vertical error bar indicates the full-width half-maximum of the PL emission. The ratio of the confinement energy, which is the PL energy in the case of HgTe, to the PL line width is between 6 and 10, which is similar to the most monodisperse CQDs presently achieved.

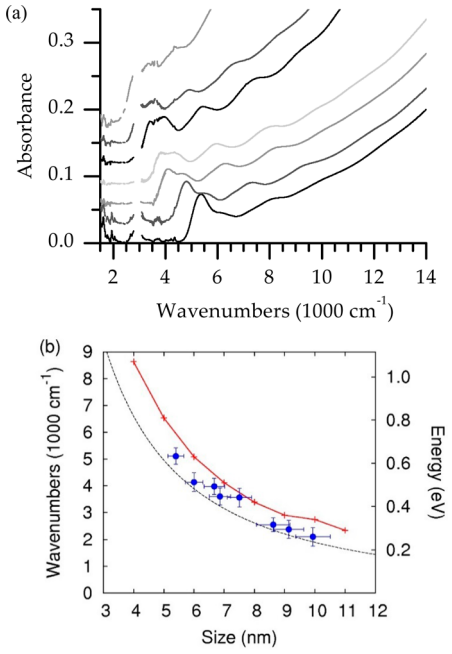

Figure 2. (a) Absorption spectra for different sizes of particles showing multiple features. The band from 2800 to 3000 cm^{-1} has been blanked due to the strong CH stretch. The full spectra are in the Supporting Information. (b) Blue dots: PL peak energy as a function of particle size as measured in TEM images. Red line and crosses: excitonic gap calculated for nanocrystals with truncated tetrahedral shape. Black dotted line: excitonic gap versus diameter calculated for spherical nanocrystals (ref 6).

To analyze the absorption data, the spectra are modeled with a sum of Gaussians and a quadratic function that captures the overall increase in absorbance at higher energies. Figure 3b shows the result of this fitting procedure with the energy of five different features as a function of the energy of the first peak. The lines are from the calculations described later.

HgTe CQDs for LWIR. To grow larger particles with a PL peak beyond 5 μm, raising the temperature above 120 °C or lengthening the reaction time was not successful, as the particles could no longer be redispersed in TCE after one precipitation. A more successful approach is to regrow the particles at 110−120 °C by dropwise addition of $HgCl_2$ and TOPTe

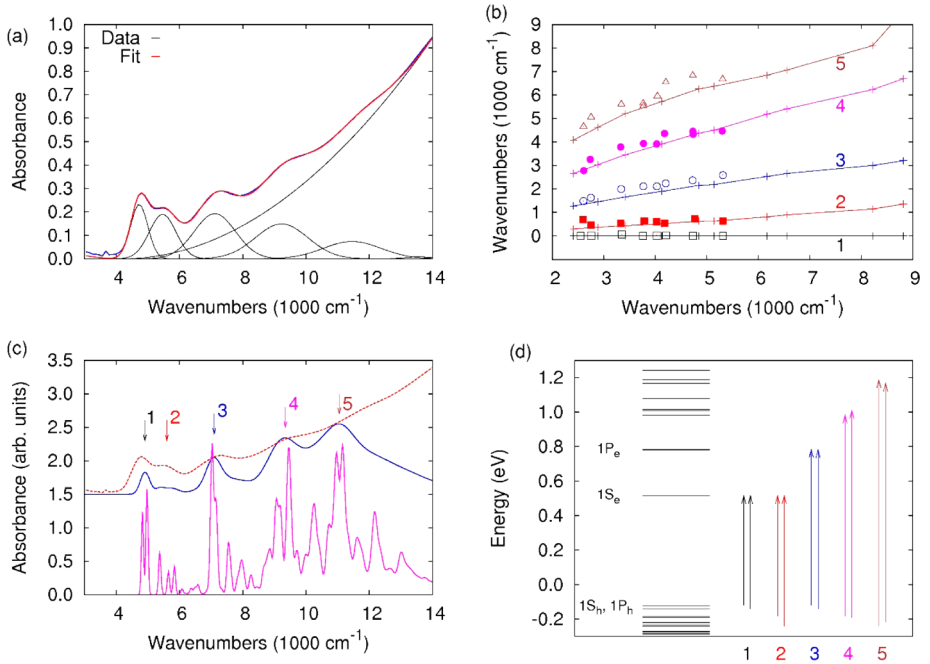

Figure 3. (a) Absorption spectrum overlaid with a fit of a sum of six Gaussians and a quadratic function (black curves). (b) Energy differences for the first five absorption features obtained from the fitting for eight different sizes. The symbols are the experimental data points, and the crosses connected by solid lines are the theoretical values. (c) Comparison between calculated (solid lines) and measured (dashed line) absorption spectra. Each transition line of the calculated spectrum is broadened by a Lorentzian function (lower curve: broadening, η, of 4 meV; upper curve: broadening increasing linearly with energy from 15 meV at 4000 cm^{-1} to 65 meV at 12000 cm^{-1}). The calculations have been done for a nanocrystal size of 6.3 nm such that the position of the lowest transition agrees with experiments. The calculated spectra are not converged above ~12000 cm^{-1} due to the limited number of excitonic states which can be computed. (d) Assignment of the experimental peaks in terms of groupings of many single hole states to the first few single electrons states.

dissolved in oleylamine. The particles then remain soluble in the quench solution using dodecanethiol ligands, and they can be precipitated with 2-propanol and redissolved in TCE. Figure 4a,b shows a TEM image of particles before and after a regrowth. There is no evidence of small particles being formed by additional nucleation. The particles are still approximately tetrahedral with rounded tips, and the facet bisector approaches ~20 nm. Typical spectra are shown in Figure 4c. The spectra of the larger particles show an edge moving to lower energy, but in contrast to the MWIR particles, they show little or no modulation and instead a nearly linearly rising absorbance. The lack of an exciton peak at the band edge comes partly from the polydispersivity and the congestion of the spectral features. In addition, as the energy is reduced, thermal occupation will diminish the optical definition of the band edge.

Photodetection. The reddest detection previously reported with colloidal quantum dots was ~7 μm at low temperature.[5] In this work, a photocurrent response is easily obtained for all the particles with an absorption edge in the MWIR. To extend the spectral range to the LWIR, there are several difficulties besides the issue of making large enough particles. Assuming undoped particles, the dark current increases as ~exp$-E_g/2kT$ leading to many orders of magnitude increases as the gap E_g decreases from near-IR to LWIR. Keeping the Fermi level at midgap is also more difficult with a small gap since changes of the surface composition can shift the

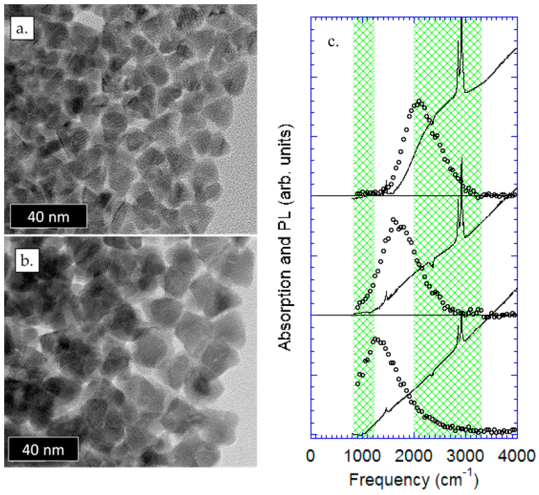

Figure 4. TEM image of samples emitting around 2000 cm^{-1} (a) and 1300 cm^{-1} (b) at room temperature. (c) Room-temperature absorption and emission spectra of HgTe quantum dot films. The solid dark lines are the absorption spectra with 4 cm^{-1} resolution and the dark open circles are the photoluminescence with 50 cm^{-1} resolution. The absorption spectra show features associated with the ligands CH stretch (~2900 cm^{-1}) and CH bend (~1500 cm^{-1}) and some uncorrected CO_2 absorption from the beam path (2350 cm^{-1}). The green shaded regions mark the LWIR and MWIR regions.

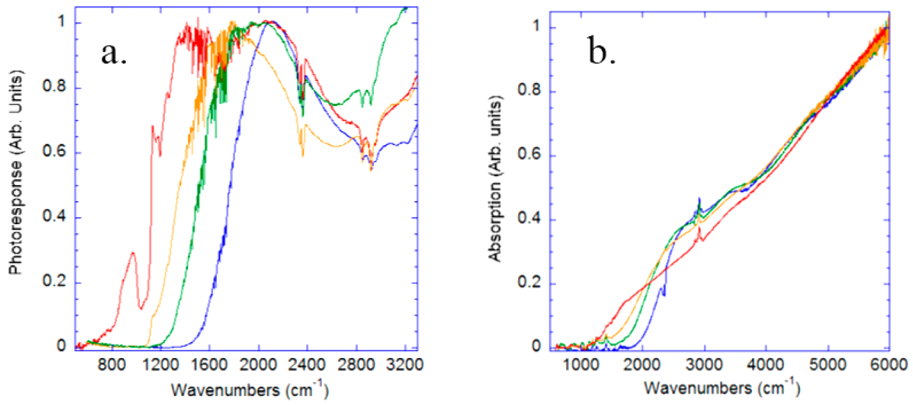

Figure 5. (a) Photocurrent response of thin films of HgTe quantum dots on a Si/SiO_2 substrate at 80 K. Samples were made with a 10 min growth at 120 °C (orange line), 110 °C (green line), and 100 °C (blue line) in order of increasing blueshift. The reddest sample (red line) was obtained with a regrowth. The spectra are normalized. (b) Room-temperature absorption spectra of thin films of the same HgTe quantum dots on a ZnSe substrate with the same color scheme as in (a). The absorption spectra are normalized at 6000 cm^{-1}.

Fermi level close to valence or conduction states[10] leading to increased dark current. In addition, nonradiative relaxation becomes much faster as the gap shrinks, as seen from the dramatic drop in photoluminescence quantum yield of the larger HgTe quantum dots.[11] At a more fundamental level, it was an open question whether the topological insulating nature of the HgTe bulk material would lead to surface states in the gap for the large quantum dots.

Figure 5a shows however the successful extension of the spectral range that now includes the LWIR, up to 12 μm (833 cm^{-1}) at 80 K. In Figure 5a, the sharp drop in signal between ~1100 and 1000 cm^{-1} is due to the ~1 μm SiO_2 layer on the Si substrate. The broad main peaks in the photoresponse spectra between 1300 and 2100 cm^{-1} are not excitonic features of the materials but are due to the constructive interference of the incident and reflected light from the Si/SiO_2 interface. A similar maximum is seen at ~4000−5000 cm^{-1} from the same effect (Supporting Information). Besides the sharp water lines (bending modes lines around 1600 cm^{-1}) and CO_2 (2350 cm^{-1}) from the path in air, one also identifies the CH stretch vibrations around 2900 cm^{-1} from the remaining ligands in the films. Spectra taken on glass and sapphire substrates with the same quantum dot samples show the influence of the substrate for these semitransparent films (Supporting Information). In particular, glass substrates lead to an artificial cutoff around 1100 cm^{-1} where the reflectivity of glass becomes high due to the Reststrahlen band. Sapphire substrates lead to a similar cutoff around 900 cm^{-1}. Figure 5b shows the absorption spectra of the corresponding films at room temperature. The redshift between the room temperature absorption edge and the 80 K photoresponse is about ~400 cm^{-1}.

Infrared detectors are characterized by their spectral response but also by their bandwidth, responsivity, and specific detectivity. HgTe colloidal quantum dot photodetectors have been characterized in the near-IR[2−4] and the mid-IR[5] previously. The results here are similar to prior results on ethanedithiol cross-linked HgTe dots in the mid-IR.[5] For a sample with an edge around 6.5 μm (~1500 cm^{-1}) at 80 K at 10 V bias, the dark current was 25 nA and the noise was 1.3×10^{-13} $AHz^{1/2}$, therefore about twice the shot noise limit. The responsivity was 1.8 mA/W and the specific detectivity was 1.3×10^9 Jones. The time response was <5 μs (Supporting Information). Higher responsivity should be obtained with thicker films and higher bias. The specific detectivity of that sample is about 2 orders of magnitude less than the commercial InSb detectors operating in this spectral range at 77 K. For a sample with detection past 12 μm at 80 K, the responsivity dropped to 0.3 mA/W, and the specific detectivity was 6.5×10^6 Jones, about 3 orders of magnitude worse than commercial detectors. That sample showed a fast response (<5 μs) as well as a slow response (ms), and its dark current remained high at ~125 μA, which likely reflect that the Fermi level is not at midgap. Therefore, although this work demonstrates the possibility of detecting long wavelength infrared with large enough HgTe quantum dots, there is much room left to improve the photocurrent response.

Electronic Structure: Theory. To understand the optical properties of the HgTe quantum dots, we performed atomistic tight-binding electronic structure calculations including excitonic effects, as described previously in detail.[6] Improved computational methods allow calculation of optical absorption spectra for dot sizes up to 12 nm. In this range of sizes, for HgTe, the excitonic effects mainly consist of rigid redshifts of the spectra.[6] Calculations were performed for regular tetrahedrons as well as tetrahedrons with rounded tips, as suggested by the TEM images. Results are shown for particles constructed by truncating all four tips of a regular tetrahedron at 30% of the original edge length. Consistent with the experimental definition of the size, the length of the bisector of each facet is the size of the

nanocrystals in the theory. Figure 2b shows the calculated excitonic gap. It slightly overestimates the experimental PL energy for truncated tetrahedrons and slightly underestimates it for spheres. The agreement is overall satisfying given the uncertainties in the experimental size and shape determination.

Figure 3 shows that the theory also reproduces the relative position and intensities of the main peaks when a sufficiently large broadening of the transition lines is assumed. It is an important prediction of the theory that each broad peak is in fact composed of many transitions which the experiment does not resolve. Furthermore, the theory shows that some parts of the spectra depend sensitively on the shape. In particular, the regular tetrahedral shape shows a much weaker second peak compared to the experimental data (Supporting Information), suggesting that the truncation breaks the selection rules.

The theory captures well the evolution of each absorption peak with size, as shown in Figure 3b, and this allows assignment of the peaks. The optical spectra can be interpreted using the single-particle energy levels calculated in tight-binding, as shown in Figure 3d for a nanocrystal size of 6.3 nm. The lowest (empty) electron state is 2-fold degenerate and is assigned to $1S_e$ following the nomenclature used for spherical dots, and this is confirmed by the plot of their wave function (Supporting Information). Similarly, the manifold of six states higher in energy can be assigned to $1P_e$ composed of two levels, $1P_e^{1/2}$ and $1P_e^{3/2}$, which are 2-fold and 4-fold degenerate, respectively. Their splitting comes from the spin−orbit coupling, and this is different from CdSe,[9] where the spin−orbit of the conduction band is negligible. Higher in energy, there are states which are approximately noted as *D*-like states. The two highest (filled) hole levels in Figure 3d are both (almost) 4-fold degenerate. The plot of their wave functions (Supporting Information) indicates that their envelope can be interpreted as $1S_h$ or $1P_h$, the $1P_h$ ($1S_h$) level being the highest one in energy for size below (above) ~9 nm. However, this assignment of the electron and hole levels must be considered with caution, especially at increasing size (Supporting Information). If the $1S_e$ ($1P_e$) wave functions are characterized by an S(P)-like envelope on the Hg atoms, their smaller component on the Te atoms cannot be classified using the same nomenclature since their amplitude is more or less constant over the nanocrystal volume for sizes about 6 nm but tends to localize near the surface for larger sizes. In addition, the envelope of the $1S_h$ states is strongly concentrated at the center of the quantum dots, especially for larger sizes, but presents small bumps close to the surface. This complex behavior comes from the unusual band structure of bulk HgTe characterized by an inverted band gap. The Γ8 band, 4-fold degenerate at Γ, is above the 2-fold degenerate Γ6 band.[12,13] Two Γ8 bands with positive dispersion form the conduction band while the two others with negative dispersion form the valence band accompanied by the Γ6 bands and the split-off Γ7 bands below in energy. In addition, the *s*- and *p*-orbital characters of these bands strongly vary with *k* around Γ, indicating a very strong coupling between the bands.[6,12] By projecting on bulk states in *k* space, we find that the electron and hole states contain multiple components from all the bands, including for Γ8 both conduction and valence bands. The multiband character of the electronic states is known to be important for small bandgap semiconductors[14] and is obviously considerable in HgTe which is a semimetal.

The mixed character (multiband and multiorbital) of the states is also reflected in the oscillator strengths of the transitions (Figure 3c,d). The lowest absorption peak (1) results from transitions from $1S_h$ and $1P_h$ to $1S_e$. Transitions from lower energy hole states to $1S_e$ explain peak 2, which is very weak in the case of regular tetrahedrons and spheres. Transitions from $1S_h$ and $1P_h$ to $1P_e$ give rise to peak 3. The fact that two absorption peaks (1 and 3) involve transitions from the same hole levels but to two electron levels, $1S_e$ and $1P_e$, is remarkable. This behavior is not found in conventional II−VI semiconductor quantum dots, like CdSe.[9] The peaks 4 and 5 are given by many transitions, mainly from the same group of lower energy hole states but to different conduction states. Once again, this confirms the mixed character of the states.

For the largest sizes, it is not possible to calculate a sufficiently converged absorption spectrum in tight-binding. However, using a set restricted to 20 electrons states and 100 hole states, we predict an excitonic gap of 1290 cm^{-1} for 16 nm truncated tetrahedrons, in good agreement with the experimental range. The density of hole states is very high for this large size, 100 states being concentrated in an energy window of 75 meV. The $1S_e-1P_e$ splitting is about 100 meV, but it is not visible in the absorption spectrum if we consider a broadening comparable to the experimental width of the PL peak (Supporting Information). As already discussed, the theory shows that some components of the electron and hole wave functions tend to localize near the surface for large sizes, but these states cannot yet be referred to as topological edge states.[15] Larger sizes will therefore be needed to see the effect of surface states on the optical properties, but it seems that surface states will not be a concern for sizes that will cover the LWIR.

CONCLUSIONS

This work demonstrates that HgTe quantum dots can be synthesized with a definition of the spectral features that is similar to the best developed colloidal quantum dot systems. The extension to quantum dots with sizes up to 20 nm is successfully achieved with a regrowth and photoconduction is now demonstrated

beyond 12 μm. Tight-binding calculations including excitonic effects provide a very good size/spectral relationship, given the uncertainty on the experimental size and shape determination for these nonspherical particles. In addition, the theory shows that the series of broad peaks in the experimental data contain multiple finer features associated with transitions from many hole states to the single electron states. Compared to usual II–VI semiconductor quantum dots, the multiband/multiorbital character of the electron and hole states is strongly enhanced by the complex inverted band structure of bulk HgTe, leading to unusual optical transition rules. Theory indicates that the topological surface states will not be a concern in the LWIR region and that they will appear at even larger sizes. While there will still be synthetic improvements possible on the colloidal quantum dots themselves, future work will have to concentrate on the surface chemistry and film processing in order to achieve higher detectivity at higher temperature.

METHODS

Synthesis. In a typical synthesis, 0.1 mmol of $HgCl_2$ is dissolved in 3 g of octadecylamine (ODA) by heating to 120 °C under vacuum for 1 h and then placed under Ar. Te (1 M, 0.1 mL) in trioctylphosphine (TOP) is then diluted with 5 mL of oleylamine, and this solution is rapidly injected into the flask. The temperature quickly drops and then partially recovers, and a growth temperature and time are chosen for the desired particle size. Growth is halted by extracting some or all of the reaction mixture to a solution of 10% (vol) dodecanethiol and ~1% TOP in tetrachloroethylene (TCE). Particles can be stored for long periods (weeks to months) in this quench solution and are purified by precipitating with methanol and redispersing in TCE for characterization.

For larger particles, CQDs emitting around 5 μm are first synthesized following the method above at 120 °C for 10 min. Equivalent volumes of 0.05 M $HgCl_2$/oleylamine and 0.05 M TOPTe/oleylamine are then added dropwise at a rate of 0.25 mL/min while the temperature is kept at 120 °C. The total amount added determines the size of the particles. To facilitate the redispersion of the larger particles after precipitation, it was found that adding dioctadecyldimethylammonium bromide (DDAB) in the quench solution and in the isopropyl alcohol used for precipitation, both at 0.01 M, was helpful.

Photoluminescence. The photoluminescence (PL) spectra of the solutions are obtained by excitation with 150 mW of a laser at 808 nm modulated at 75 kHz where the collected luminescence passes through a home-built step-scan Michelson interferometer and onto an MCT detector with a 11.5 μm cutoff and is measured with a lock-in amplifier. Photoluminescence of films is taken with the same instrument, where films are dried on a polished aluminum substrate and rinsed with ethanol to remove unbound organics.

Photocurrent Detection. Films are deposited on interdigitated electrode substrates. The electrodes are 5 μm wide, with 20 μm gaps, and cover a 1 × 1 mm region. The electrodes are 5 nm Ti and 10 nm Pd. Substrates tested are Si/SiO_2, glass, and sapphire. The SiO_2 film on Si has a thickness of 1.0 μm which gives surface maxima of the electromagnetic field strength around 1500 and 5000 cm^{-1}, which is beneficial when measuring the photoresponse of the reddest samples. The HgTe particle films are drop cast from the clean TCE solution. For the initial experiments, the films were cross-linked in a 2% ethanedithiol solution in ethanol, and all film handling and processing was done in a glovebox. This was necessary as air exposure during and after dithiol cross-linking leads to unintentional doping evidenced by a nonmonotonic change of the film resistance upon cooling, resulting in a larger dark current.[16] It was reasoned that adding HCl would diminish the oxidation of the dithiols to disulfides while the Cl^- ions may also passivate the exposed mercury atoms on the surface of the dots protecting against oxidation, and it was found that treating the films in air in 2% ethanedithiol and 2% HCl in ethanol for ~10 s and rinsing with ethanol led to similar results as treatment in the glovebox. With this preparation, the resistance always increases upon cooling in a monotonic fashion. All data reported are therefore for films completely processed in air. The films can be made thicker by repeating the process two to three times. The films are thin, semitransparent, and of a thinkness of a few hundred nanometers. The thickness is adjusted so that the room-temperature resistance is in the 10–100 kΩ range and is therefore not optimized for complete light absorption or maximum responsivity. The sample is clamped on a copper coldfinger in a chamber with a ZnSe window that is evacuated and cooled by liquid nitrogen to a temperature of 80 K.

A Nicolet 550 FTIR spectrometer is used to measure the photocurrent spectra. The internal glow bar light source is directed to the outer port and imaged on the sample with a 5 cm focal length parabolic mirror. A scanning speed of ~1 cm/s is typically used (corresponding to ~0.1 ms for the interferogram peak).

For spectra shown in Figure 5a, the sample is biased with a 9 V battery in series with a selectable load resistance matched to the sample resistance, and the voltage across the sample is amplified by an SR570 AC voltage amplifier and fed into the spectrometer input signal. However, this limits the response speed when the sample resistance is in excess of a few MΩ. A faster response is achieved by using a Femto DLPCA-200 current amplifier before the SR570 voltage amplifier.

As an example, for the reddest sample in the LWIR shown in Figure 5a, the room-temperature resistance was 30 kΩ, and it increased to 3 MΩ at 80 K. The load resistance was 1 MΩ. With a gain of 200, the interferogram peak amplitude was ~6 V with the noise in the 10 mV range, and it was easily detected.

Absorption Spectra of Films. Thin films (~100 nm thick) are dried on a 1 in. long and 3 mm thick ZnSe attenuated total reflectance (ATR) plate with 45° bevels. The dried films are then rinsed with ethanol (Figure 4c) or processed with the cross-linking solutions and rinsed with ethanol (Figure 5b), and the spectra are measured with a Nicolet 550 FTIR.

Tight-Binding Calculations. The single-particle tight-binding Hamiltonian matrix is written in a basis of 20 orbitals ($sp^3d^5s^*$ for each spin orientation) on each Hg or Te atom as a function of parameters that have been obtained by fitting to two reference band structures: (1) close to the Fermi level, on the k.p. band structure of ref 17; (2) elsewhere, on the band structure of ref 18. obtained using a quasi-particle self-consistent GW approximation in a hybrid scheme. The surfaces of the nanocrystals are saturated by pseudohydrogen atoms in order to avoid surface states. Because of the large size of the systems studied, only near-gap eigenstates are calculated using the numerical methods described in ref 19.

To account for the excitonic effects on the optical properties, we calculate the excitonic states using a configuration-interaction (CI) method.[20–22] In a first step, we calculate the self-energy corrections to the single-particle energies induced by the dielectric polarization of the quantum dot following the injection of the separate electron and hole. In a second step, the screened electron–hole coulomb interaction is introduced into the excitonic Hamiltonian which is written in the basis of Slater determinants built from the tight-binding single-particle states. The oscillator strengths for the optical transitions are computed using the eigenstates of the excitonic Hamiltonian. The optical spectra are calculated including local-field effects. For the sake of comparison with experiments, each optical transition line is

broadened using a Lorentzian function $L(\omega) = (\eta)/(\omega^2 + \eta^2)$ where η is a parameter. Full details on the methodology are given in ref 6.

Conflict of Interest: The authors declare no competing financial interest.

Acknowledgment. This work was supported by the US National Science Foundation (NSF; Grant No. DMR-1104755). The authors made use of shared facilities supported by the NSF MRSEC Program under DMR-0820054.

Supporting Information Available: Details of the calculations and example plots of electron and hole wave functions, absorption spectra with and without the molecular vibration bands, photoresponse on different substrates, detectivity, responsivity, and bandwidth data. This material is available free of charge *via* the Internet at http://pubs.acs.org.

REFERENCES AND NOTES

1. Rogalski, A. Progress in Focal Plane Array Technologies. *Prog. Quantum Electron.* **2012**, *36*, 342–473.
2. Rauch, T.; Boberl, M.; Tedde, S. F.; Furst, J.; Kovalenko, M. V.; Hesser, G. N.; Lemmer, U.; Heiss, W.; Hayden, O. Near-Infrared Imaging with Quantum-Dot-Sensitized Organic Photodiodes. *Nature Phot.* **2009**, *3*, 332–336.
3. Boberl, M.; Kovalenko, M. V.; Gamerith, S.; List, E. J. W.; Heiss, W. Inkjet-Printed Nanocrystal Photodetectors Operating up to 3 μm Wavelengths. *Adv. Mater.* **2007**, *19*, 3574–3578.
4. Chen, M.; Yu, H.; Kershaw, S. V.; Xu, H.; Gupta, S.; Hetsch, F.; Rogach, A. L.; Zhao, N. Fast, Air-Stable Infrared Photodetectors based on Spray-Deposited Aqueous HgTe Quantum Dots. *Adv. Funct. Mater.* **2014**, *24*, 53–59.
5. Luillier, E.; Keuleyan, S.; Guyot-Sionnest, P. Mid-IR Colloidal Nanocrystals. *Chem. Mater.* **2013**, *25*, 1272–1282.
6. Allan, G.; Delerue, C. Tight-Binding Calculations of the Optical Properties of HgTe Nanocrystals. *Phys. Rev. B* **2012**, *86*, 165437.
7. Keuleyan, S.; Lhuillier, E.; Guyot-Sionnest, P. Synthesis of Colloidal HgTe Quantum Dots for Narrow Mid-IR Emission and Detection. *J. Am. Chem. Soc.* **2011**, *133*, 16422–16424.
8. Keuleyan, S. Mid-Infrared Mercury Chalcogenide Colloidal Quantum Dots. Ph.D. Thesis, The University of Chicago, 2013.
9. Norris, D. J.; Bawendi, M. G. Measurement and Assignment of the Size-Dependent Optical Spectrum in CdSe Quantum Dots. *Phys. Rev. B* **1996**, *53*, 16338–16346.
10. Jeong, K. S.; Deng, Z.; Keuleyan, S.; Liu, H.; Guyot-Sionnest, P. Air-Stable n-Doped Colloidal HgS Quantum Dots. *J. Phys. Chem. Lett.* **2014**, *5*, 1139–1143.
11. Keuleyan, S.; Kohler, J.; Guyot-Sionnest, P. Photoluminescence of Mid-Infrared HgTe Colloidal Quantum Qots. *J. Phys. Chem. C* **2014**, *118*, 2749–2753.
12. Svane, A.; Christensen, N. E.; Cardona, M.; Chantis, A. N.; van Schilfgaarde, M.; Kotani, T. Quasiparticle Band Structures of β-HgS, HgSe, and HgTe. *Phys. Rev. B* **2001**, *84*, 205205.
13. Nicklas, J. W.; Wilkins, J. W. Accurate Electronic Properties for (Hg,Cd)Te Systems Using Hybrid Density Functional Theory. *Phys. Rev. B* **2011**, *84*, 121308.
14. Richard, T.; Lefebvre, P.; Mathieu, H.; Allègre, J. Effects of Finite Spin-Orbit Splitting on Optical Properties of Spherical Semiconductor Quantum Dots. *Phys. Rev. B* **1996**, *53*, 7287–7298.
15. Pankratov, O. A.; Pakhomov, S. V.; Volkov, B. A. Supersymmetry Heterojunctions: Band Inverting Contact on the Basis of $Pb_{1-x}Sn_xTe$ and $Hg_{1-x}Cd_xTe$. *Solid State Commun.* **1987**, *61*, 93–96.
16. Lhuillier, E.; Keuleyan, S.; Zolotavin, P.; Guyot-Sionnest, P. Mid-Infrared HgTe/As_2S_3 Field Effect Transistors and Photodetectors. *Adv. Mater.* **2013**, *25*, 137–141.
17. Man, P.; Pan, D. S. Infrared Absorption in HgTe. *Phys. Rev. B* **1991**, *44*, 8745–8758.
18. Svane, A.; Christensen, N. E.; Cardona, M.; Chantis, A. N.; van Schilfgaarde, M.; Kotani, T. Quasiparticle Band Structures of β-HgS, HgSe, and HgTe. *Phys. Rev. B* **2001**, *84*, 205205.
19. Niquet, Y. M.; Delerue, C.; Allan, G.; Lannoo, M. Method for Tight-Binding Parametrization: Application to Silicon Nanostructures. *Phys. Rev. B* **2000**, *62*, 5109–5116.
20. Delerue, C.; Lannoo, M. *Nanostructures: Theory and Modeling*; Springer: New York, 2004.
21. Martin, E.; Delerue, C.; Allan, G.; Lannoo, M. Theory of Excitonic Exchange Splitting and Optical Stokes Shift in Silicon Nanocrystallites: Application to Porous Silicon. *Phys. Rev. B* **1994**, *50*, 18258–18267.
22. Franceschetti, A.; Fu, H.; Wang, L. W.; Zunger, A. Many-Body Pseudopotential Theory of Excitons in InP and CdSe Quantum Dots. *Phys. Rev. B* **1999**, *60*, 1819–1829.